Doppler System Phase Transfer Functions for a System With an X-Band Uplink and X-Band and S-Band Downlinks

M. A. Koerner
Telecommunications Systems Section

A new DSN RF system is being developed that can transmit at X-band and receive at both X-band and S-band. End-to-end tests are planned to measure the phase stability of this system. This article derives equations for the phase transfer functions between the error sources in the system and the X-band and S-band doppler extractor outputs. This analysis considers both test modes, using a test translator, and actual spacecraft tracking where the spacecraft is at some distance from the DSN station. The results indicate that the proposed end-to-end tests will not accurately reflect the error that will occur during actual spacecraft tracking.

I. Introduction

The next step in the evolution of radio links for planetary spacecraft is the use of an X-band frequency (nominally 7162.3125 MHz) instead of an S-band frequency (nominally 2113.3125 MHz) for the uplink. Experimental X-band receivers will be flown on Galileo and Venus Radar Mapper. A new DSN RF system is being developed that can transmit at X-band and receive at both X-band and S-band.

One justification for an X-band uplink is increased doppler measurement accuracy, primarily for radio-science experiments to measure gravitational waves. The two largest sources of doppler measurement error in the present system, which uses an S-band uplink, are those caused by charged particles, in both the Earth's ionosphere and the interplanetary plasma, and receiver thermal noise. A new method of extracting frequency estimates from doppler phase data would make thermal noise effects negligible as long as no receiver cycle slips occur. Use of an X-band uplink should reduce the doppler measurement error caused by the Earth's ionosphere and the interplanetary plasma by at least an order of magnitude. Thus, use of an X-band uplink yields the potential for substantial improvement in doppler system accuracy.

A critical question is the phase stability of the ground radio equipment. Considerable care has been taken in the design of this equipment, and end-to-end tests, using test translators instead of a transponder, will be made to verify the phase stability of the DSN RF system hardware. However, test results with a test translator may differ significantly from those that would be observed with a transponder at a significant distance from the DSN station.

The analysis presented here determines the phase transfer function between each of a number of phase error sources in

the DSN RF system equipment and the X-band and S-band doppler extractor outputs. Both test configurations, using test translators, and the actual tracking configuration with a transponder and finite two-way time delay are considered. Comparing the phase transfer functions for the test configurations with those for the actual tracking configuration will yield considerable qualitative insight into which phase error sources will be accurately measured by the planned end-to-end measurements and which will not be accurately measured by these tests. These phase transfer functions can also be used in a future analysis to quantitatively calculate the contribution of each phase error source, given an Allen variance curve or phase noise power spectrum for the error source, to the doppler system inaccuracy.

A number of phase error sources are considered in this analysis. Θ_A is the phase of the hydrogen maser's 100 MHz output. Since both the X-band and S-band doppler extractor outputs analyzed in this article are 1 MHz biased doppler, the $0.01\,\Theta_A$ terms in the equations for the doppler extractor outputs are the 1.0 MHz bias. All other terms in Θ_A represent error. Other sources in the transmitting path are the phase error ϕ_{CC}, introduced by the temperature compensated cable between the hydrogen maser and the antenna-mounted equipment; the phase error ϕ_{UC}, introduced by the uncompensated cable between the exciter frequency synthesizer in the control room and the antenna-mounted equipment; the phase error ϕ_{ES}, introduced by the exciter frequency synthesizer; the phase error ϕ_{EM}, contributed by the exciter modulator; and the phase error ϕ_{PA}, contributed by the RF power amplifier. X-band receiver phase errors are the phase error ϕ_{XV}, contributed by the X-band receiver VCO; and the phase error ϕ_{XS}, contributed by the X-band receiver frequency synthesizer. S-band receiver phase errors are the phase error ϕ_{SV}, contributed by the S-band receiver VCO; and the phase error ϕ_{SS}, contributed by the S-band receiver frequency synthesizer.

A very simplified block diagram of the DSN RF system is shown in Fig. 1, which also shows the spacecraft transponder. The analytical models for the blocks shown in Fig. 1 are discussed in Section II. The results of combining the analytical models discussed in Section II are shown in Sections III and IV. Sections III and IV show the transfer function between each error source and the X-band and S-band doppler extractor outputs. In each case, the transfer functions for the test configurations are compared with those for the actual tracking configuration. Section V presents the report's conclusions.

II. System Elements

This section presents the analytical model and transfer functions for the major elements of the (X/X,X/S) system. The numbers printed on the figures associated with this section are the frequencies in MHz at various points of the (X/X,X/S) system, given that the uplink frequency is 7162.3125 MHz, the X-band downlink frequency is 8415 MHz, and the S-band downlink frequency is 2295 MHz. In addition, the symbol Θ with various subscripts is used to denote the total signal phase at various points in the system, and the symbol ϕ with appropriate subscripts is used for the phase noise or phase instabilities in the system.

The symbols M_E, M_X, and M_S are introduced in this section to denote the exciter, X-band RF receiver, and S-band RF receiver frequency synthesizer multiplication factors. These multiplication factors are adjusted to change the transmitter, X-band receiver and S-band receiver frequencies. The Appendix derives the relationships between M_E, M_X, and M_S and the transmitter and receiver frequencies and the interrelationship between M_E, M_S, and M_X

A. Exciter RF Frequency Generator

The analytical model for the exciter RF frequency generator is shown in Fig. 2. Θ_A is the phase of the 100 MHz hydrogen maser frequency standard output. The maser and the exciter frequency synthesizer, which performs the "$\times M_E$" frequency multiplication, are located in the DSN station control room. The phase error ϕ_{ES} rerpesents the phase error contribution of the exciter frequency synthesizer.

The rest of the equipment modeled in Fig. 2 is antenna-mounted. The 41.39453125 MHz (nominal) output of the frequency synthesizer is transmitted to the antenna via an uncompensated cable. $M_E\,\phi_{UC}$ represents the phase instability of this cable, where ϕ_{UC} represents the phase instability normalized to 100 MHz. The 100 MHz maser output is sent to the antenna via a compensated cable, which introduces a phase error ϕ_{CC}. On the antenna the "$\times$ 16" multiple of the uncompensated cable output is added (in phase) to the "$\times$ 65" multiple of the compensated cable output to yield the RF signal phase Θ_D. The outputs, Θ_B and Θ_C, of the uncompensated and compensated cables are also used by the doppler extractors.

From Fig. 2,

$$\Theta_B = M_E\,(\phi_{UC} + \Theta_A) + \phi_{ES} \tag{1}$$

$$\Theta_C = \phi_{CC} + \Theta_A \tag{2}$$

and

$$\Theta_D = (65 + 16\,M_E)\,\Theta_A + 16\,M_E\,\phi_{UC} + 65\,\phi_{CC} + 16\,\phi_{ES} \tag{3}$$

B. Transmitter

In the transmitter analytical model, ϕ_{EM} will be used to denote the phase error introduced by the exciter-modulator and ϕ_{PA} to denote that introduced by the RF power amplifier. The exciter-modulator/power amplifier element incorporates a phase compensation loop. The feedback point for this loop may be either the exciter-modulator output or the RF power amplifier output. Thus, two analytical models are required for the exciter-modulator/power amplifier element. Figure 3 shows the analytical model for feedback from the exciter output. Figure 4 shows the analytical model for feedback from the power amplifier output. Other than the feedback point for the phase compensation loop, the two analytical models are identical.

If feedback is taken from the exciter output, the exciter output will be

$$\Theta_E = \Theta_D + [1 - H(s)]\ \phi_{EM} \tag{4}$$

and the power amplifier output will be

$$\Theta_F = \Theta_D + [1 - H(s)]\ \phi_{EM} + \phi_{PA} \tag{5}$$

where

$$H(s) = \left(\frac{k}{k+1}\right)\frac{1}{1+\frac{\tau}{k+1}s} \tag{6}$$

$$1 - H(s) = \left(\frac{1}{k+1}\right)\frac{1+\tau s}{1+\frac{\tau}{k+1}s} \tag{7}$$

and

$$k = k_D G_A k_\phi \tag{8}$$

is the gain of the phase compensation loop.

If feedback is taken from the power amplifier output, the exciter output will be

$$\Theta_E = \Theta_D + [1 - H(s)]\ \phi_{EM} + H(s)\,\phi_{PA} \tag{9}$$

and the power amplifier output will be

$$\Theta_F = \Theta_D + [1 - H(s)]\ (\phi_{EM} + \phi_{PA}) \tag{10}$$

Figure 5 shows sketches of $|H(s)|$ and $|1 - H(s)|$ as a function of frequency.

$$f_L = \frac{1}{(2\pi\tau)} \tag{11}$$

and

$$f_H = (k+1)\,f_L \tag{12}$$

Since $k_D = 0.9 \times 10^{-3}$ V/deg, $G_A = 1220$, and $k = 47$ deg/V, k is equal to 51.606. τ may be equal to either 4 s or 0.528×10^{-2} s. For $\tau = 4$ s, $f_L = 0.040$ Hz and $f_H = 2.09$ Hz. For $\tau = 0.528 \times 10^{-2}$ s, $f_L = 30.142$ Hz and $f_H = 1585.70$ Hz.

Which phase compensation loop mode is used will be determined by the spectral characteristics of the signal to be phase-modulated onto the uplink carrier. Since the uplink phase modulator is inside the transmitter phase compensation loop, uplink command or ranging modulation will be filtered by the $1 - H(s)$ response of the loop. If the phase modulation has significant components at frequencies below 1585.70 Hz, the narrowband ($\tau = 4$ s) mode must be used. For example, the narrowband mode must be used for systems using a Voyager-type command system. For systems whose uplink phase modulation has no significant spectral components below 1585.70 Hz, the wideband mode can be used. This results in better transmitter phase noise compensation and, consequently, in better doppler tracking accuracy. Systems that use the NASA standard command system or that operate in a mode where uplink command modulation is not currently required can use the wideband mode.

C. Test Translators

Two test translators are provided in the exciter/receiver system. One generates an X-band downlink signal (8415 MHz nominal) from the X-band uplink signal (7162.3125 MHz nominal). The other generates an S-band downlink signal (2295 MHz nominal) from the X-band uplink signal. The appropriate references for the frequency translation are provided by the X-band and S-band doppler extractors. Analytical models for the two test translators are shown in Figs. 6 and 7. Using the notation shown in these figures, the X-band test translator output is

$$\Theta_I = \Theta_H + \Theta_G \tag{13}$$

where Θ_H is the X-band test translator input and Θ_G is the (nominally 1252.6875 MHz) reference from the X-band doppler extractor, and the S-band test translator output is

$$\Theta_L = \Theta_K - \Theta_J \tag{14}$$

where Θ_K is the S-band test translator input and Θ_J is the (nominally 4867.3125 MHz) reference signal from the S-band doppler extractor.

D. X-Band Receiver Analytical Model

Figure 8 shows the analytical model for the X-band receiver. The first down-converter and the "X 81" frequency multiplier are antenna mounted. The remainder of the equipment is located in the control room. After the first down-conversion to 315 MHz (nominal), the "X 50" multiple of the difference between the 48.3 MHz (nominal) output of the X-band receiver synthesizer and the 21 MHz VCO output is used to translate the received signal to 1050 MHz. Two additional stages of down-conversion, to 50 MHz and 10 MHz, precede the phase detector, which operates at 10 MHz. The reference signals for these two down-converters and the phase detector are derived from the 100 MHz hydrogen maser frequency standard. The standard also drives the receiver frequency synthesizer.

Three sources of phase noise are shown in Fig. 8 in addition to the phase noise on the hydrogen maser frequency reference. As noted previously ϕ_{CC} is the phase instability in the temperature-compensated cable used to carry the 100 MHz reference signal up to the antenna-mounted equipment. ϕ_{XS} is the phase noise contributed by the X-band receiver frequency synthesizer. ϕ_{XV} is the phase noise contributed by the X-band receiver VCO.

Analyzing Fig. 8, if we define

$$H_X(s) = \frac{1 + \tau_2 s}{1 + \left(\tau_2 + \frac{1}{k_L}\right)s + \frac{\tau_1}{k_L} s^2} \tag{15}$$

where

$$k_L = 50\,\alpha\, k_D k_F k_V, \tag{16}$$

the phase of the X-band receiver output is

$$\Theta_N = H_X(s)\,(\Theta_M - 81\,\phi_{CC}) + [1 - H_X(s)]\;50\,\phi_{XV} - [1 - H(s)]50\,\phi_{XS} - [50\,M_X + (70.5 - 50\,M_X)\,H_X(s)]\;\Theta_A \tag{17}$$

where Θ_M is the phase of the X-band receiver input.

E. S-Band Receiver Analytical Model

Figure 9 shows the analytical model for the S-band receiver. The first down-converter and the "X 20" frequency multiplier are antenna-mounted. The remainder of the equipment is located in the control room.

The block diagram of the S-band receiver is very nearly identical to that of the X-band receiver. The initial down-conversion uses a "X 20" multiple of the 100 MHz hydrogen maser reference signal. Thus, for a 2295 MHz received signal, the initial down-conversion is to 295 MHz. This IF frequency requires the S-band receiver frequency synthesizer output to be at 47.9 MHz. Otherwise, the block diagrams of the X-band and S-band receivers are identical.

Analyzing Fig. 9, if we define

$$H_S(s) = \frac{1 + \tau_2 s}{1 + \left(\tau_2 + \frac{1}{k_L}\right)s + \frac{\tau_1}{k_L} s^2} \tag{18}$$

where

$$k_L = 50\,\alpha\, k_D k_F k_V, \tag{19}$$

$$\Theta_P = H_S(s)\,(\Theta_O - 20\,\phi_{CC}) + [1 - H_S(s)]\,50\,\phi_{SV} - [1 - H_S(s)]\;50\,\phi_{SS} - [50\,M_S + (9.5 - 50\,M_S)\,H_S(s)]\;\Theta_A \tag{20}$$

Note that the values of τ_1, τ_2, k_L, α, k_D, k_F, and k_V for the S-band receiver may not be the same as those for the X-band receiver.

F. X-Band Doppler Extractor

Figure 10 shows the analytical model for the X-band doppler extractor. Input phases are Θ_B, Θ_C, and Θ_D from the exciter RF frequency generator, the hydrogen maser frequency standard phase Θ_A, and the phase Θ_N of the X-band receiver output. Note that the phase of the "X 10480/749" frequency multiplier output is the phase Θ_G of the reference signal used by the X-band test translator.

Analyzing Fig. 10, the phase of the reference signal used by the X-band test translator is

$$\Theta_G = \left(\frac{2096}{749}\right)\Theta_B + \left(\frac{8515}{749}\right)\Theta_C \tag{21}$$

and the phase of the X-band doppler extractor output is

$$\Theta_Q = \Theta_N - 10.49\,\Theta_A - \left(16 + \frac{2096}{749}\right)\Theta_B + \left(16 - \frac{8515}{749}\right)\Theta_C \tag{22}$$

G. S-Band Doppler Extractor

Figure 11 shows the analytical model for the S-band doppler extractor. Input phases are Θ_B and Θ_C from the exciter RF frequency generator, the hydrogen maser frequency standard phase Θ_A, and the phase Θ_P of the S-band receiver output. Note that the phase of the "X 40720/749" frequency multipler output is the phase Θ_J of the reference signal used by the S-band test translator.

In the analysis of Fig. 11, the phase of the reference signal used by the S-band test translator is

$$\Theta_J = \left(\frac{8144}{749}\right)\Theta_B + \left(\frac{33085}{749}\right)\Theta_C \tag{23}$$

and the phase of the S-band doppler extractor output is

$$\Theta_R = \Theta_P - 10.49\,\Theta_A - \left(16 - \frac{8144}{749}\right)\Theta_B - \left(45 - \frac{33085}{749}\right)\Theta_C \tag{24}$$

III. X/X Transfer Functions

A. Testing

If the system is in the test mode, the X-band receiver input is equal to the X-band test translator output. Thus,

$$\Theta_M = \Theta_I = \Theta_H + \Theta_G \tag{25}$$

Switching in the transmitter permits the test translator input to be either the RF power amplifier output ($\Theta_H = \Theta_F$) or the exciter output ($\Theta_H = \Theta_E$). Futhermore, additional switching permits the feedback point for the transmitter phase-compensation loop to be taken from either the RF power amplifier output or the exciter output. For phase-compensation loop feedback from the power amplifier output, Θ_E and Θ_F are given by Eqs. (9) and (10). For feedback from the exciter output, Θ_E and Θ_F are given by Eqs. (4) and (5).

Combining the appropriate relationship between the X-band test translator input Θ_H and either Θ_E or Θ_F and the transfer functions derived in Section 2 of this report yields

$$\Theta_Q = 0.01\,\Theta_A + \phi_X \tag{26}$$

where Θ_Q is the X-band doppler extractor output, 0.01 Θ_A is the 1 MHz bias, and the X-band doppler phase error is

$$\begin{aligned}\phi_X = {} & \left[-(65 + 16\,M_E)\left(\frac{880}{749}\right) + (70.5 - 50\,M_X)\right] \\ & \times [1 - H_X(s)]\,\Theta_A - 16\left(\frac{880}{749}\right)M_E\,[1 - H_X(s)]\,\phi_{UC} \\ & + \left(81 - 65 \cdot \frac{880}{749}\right)[1 - H_X(s)]\,\phi_{CC} \\ & - 16\left(\frac{880}{749}\right)[1 - H_X(s)]\,\phi_{ES} \\ & + [1 - H_X(s)]\,50\,(\phi_{XV} - \phi_{XS}) \\ & + H_X(s)\,\phi_T\end{aligned} \tag{27}$$

The net transmitter phase error is

$$\left.\begin{aligned}\phi_T &= [1 - H(s)]\,(\phi_{EM} + \phi_{PA}), && O = PA, FB = PA \\ &= [1 - H(s)]\,\phi_{EM}, && O = E, FB = E \\ &= [1 - H(s)]\,\phi_{EM} + \phi_{PA} && O = PA, FB = E \\ &= [1 - H(s)]\,\phi_{EM} + H(s)\,\phi_{PA}, && O = E, FB = PA\end{aligned}\right\} \tag{28}$$

In Eq. (28), $O = PA$ denotes output from the power amplifier, $O = E$ denotes output from the exciter, $FB = PA$ denotes feedback from the power amplifier output, and $FB = E$ denotes feedback from the exciter output.

B. Actual Spacecraft Tracking

During actual spacecraft tracking, the X-band receiver input will be

$$\Theta_M = \left(\frac{880}{749}\right)H_T(s)\exp(-\tau s)\,\Theta_F \tag{29}$$

where $H_T(s)$ is the spacecraft receiver transfer function, τ is the two-way group delay and Θ_F is the RF power amplifier output. Note that error sources in the spacecraft and the ground receiving system thermal noise have been neglected.

Combining Eq. (29) and the transfer functions derived in Section II yields, for this case,

$$\phi_X = \left\{ -(65 + 16 M_E)\left(\frac{880}{749}\right)[1 - H_T(s) H_X(s) \exp(-\tau s)] + (70.5 - 50 M_X)[1 - H_X(s)] \right\} \Theta_A$$

$$- 16\left(\frac{880}{749}\right) M_E [1 - H_T(s) H_X(s) \exp(-\tau s)] \phi_{UC}$$

$$+ \left\{ 81 [1 - H_X(s)] - 65\left(\frac{880}{749}\right) \times [1 - H_T(s) H_X(s) \exp(-\tau s)] \right\} \phi_{CC}$$

$$- 16\left(\frac{880}{749}\right)[1 - H_T(s) H_X(s) \exp(-\tau s)] \phi_{ES}$$

$$+ [1 - H_X(s)]\, 50 (\phi_{XV} - \phi_{XS})$$

$$+ \left(\frac{880}{749}\right) H_T(s) H_X(s) \exp(-\tau s) \phi_T \qquad (30)$$

where

$$\phi_T = [1 - H(s)] (\phi_{EM} + \phi_{PA}), \quad FB = PA$$

$$= [1 - H(s)] \phi_{EM} + \phi_{PA}, \quad FB = E \qquad (31)$$

where $FB = PA$ indicates the feedback is taken from the power amplifier output and $FB = E$ indicates the feedback is taken from the exciter output. Note that for the configurations possible during actual spacecraft tracking, Eqs. (28) and (31) are the same.

In either the test or tracking configurations, ϕ_X is the total X-band doppler phase error. Compare Eq. (27) for ϕ_X during testing with Eq. (30) for ϕ_X during actual spacecraft tracking. Note that the error contribution of some terms will be much greater in the tracking configuration than in a test configuration. One difference is in the transfer functions for Θ_A, ϕ_{UC}, ϕ_{CC}, and ϕ_{ES}. In a test configuration the appropriate transfer function is, from Eq. (27), $1 - H_X(s)$. In the tracking configuration, the appropriate transfer function is from Eq. (30), either $1 - H_X(s)$, $1 - H_T(s) H_X(s) \exp(-\tau s)$, or some weighted sum of these two transfer functions.

Assume $H_T(s) = 1$ and $H_X(s) = 1$ over the frequency band occupied by the error sources. During testing the error contributions from Θ_A, ϕ_{UE}, ϕ_{CC}, and ϕ_E would be zero. During actual spacecraft tracking, however,

$$1 - H_T(i\omega) H_X(i\omega) \exp(-i\omega\tau) = 1 - \exp(-i\omega\tau)$$

$$= 2i \sin(\omega\tau/2) \exp(-i\omega\tau/2) \qquad (32)$$

For large τ (large spacecraft distance), this transfer function has significant low frequency response. Thus, the doppler phase errors caused by Θ_A, ϕ_{UC}, ϕ_{CC}, and ϕ_{ES} may be much greater during actual spacecraft tracking than during testing. However, the doppler phase errors caused by the X-band receiver phase noise, ϕ_{XV} and ϕ_{XS}, will be the same during tests as during actual spacecraft tracking. Thus, doppler system tests will accurately measure the X-band doppler system phase errors resulting from ϕ_{XV} and ϕ_{XS} but not those resulting from Θ_A, ϕ_{UC}, ϕ_{CC}, and ϕ_{ES}.

For the same transmitter mode of operation, the transmitter contribution to the X-band doppler phase noise should be somewhat greater during actual tracking than during testing. Comparison of Eqs. (27) and (30) shows that the transmitter contribution to X-band doppler phase noise is $H_X(s)\phi_T$ during testing and $(880/749) H_T(s) H_X(s) \exp(-\tau s) \phi_T$ during actual tracking. Thus, if one assumes $H_T(s) = 1$ over the frequency band of interest, the Allen variance of the transmitter contribution to X-band doppler phase noise will be a factor of $(880/749)^2$ greater during actual spacecraft tracking than during testing with the same transmitter mode.

IV. X/S Transfer Functions

A. Testing

If the system is in the test mode, the S-band receiver input is equal to S-band test translator output. Thus

$$\Theta_R = \Theta_L = \Theta_K - \Theta_J \qquad (33)$$

Thus, following the same approach used for the X-band doppler phase, the S-band doppler phase will be

$$\Theta_R = 0.01\, \Theta_A + \phi_S \qquad (34)$$

where

$$\phi_S = \left[-(65 + 16 M_E)\left(\frac{240}{749}\right) + (9.5 - 50 M_S)\right][1 - H_S(s)] \Theta_A$$

$$- 16\left(\frac{240}{749}\right) M_E [1 - H_S(s)] \phi_{UC}$$

$$- \left(65 \cdot \frac{240}{749} - 20\right)[1 - H_S(s)] \phi_{CC}$$

$$- 16\left(\frac{240}{749}\right)[1 - H_S(s)]\ \phi_{ES}$$

$$+ [1 - H_S(s)]\ 50\,(\phi_{SV} - \phi_{SS})$$

$$+ H_S(s)\ \phi_T \qquad (35)$$

is the S-band doppler phase error, and ϕ_T is as specified in Eq. (28).

B. Actual Spacecraft Tracking

During actual spacecraft tracking, the S-band receiver input will be

$$\Theta_O = \left(\frac{240}{749}\right) H_T(s) \exp(-\tau s)\ \Theta_F \qquad (36)$$

where $H_T(s)$ is the spacecraft receiver transfer function, τ is the two-way group delay and Θ_F is the X-band RF power amplifier output. Note that error sources in the spacecraft and the ground receiving system thermal noise have been neglected.

Combining Eq. (36) and the transfer functions derived in Section II yields, for this case,

$$\phi_S = \left\{-(65 + 16\,M_E)\left(\frac{240}{749}\right)[1 - H_T(s)\,H_S(s)\exp(-\tau s)]\right.$$

$$\left. + (9.5 - 50\,M_S)\,[1 - H_S(s)]\right\}\Theta_A$$

$$- 16\,M_E\left(\frac{240}{749}\right)[1 - H_T(s)\,H_S(s)\exp(-\tau s)]\ \phi_{UC}$$

$$- \left\{65\left(\frac{240}{749}\right)[1 - H_T(s)\ H_S(s)\exp(-\tau s)]\right.$$

$$\left. - 20\,[1 - H_S(s)]\right\}\phi_{CC}$$

$$- 16\left(\frac{240}{749}\right)[1 - H_T(s)\,H_S(s)\exp(-\tau s)]\ \phi_{ES}$$

$$+ [1 - H_S(s)]\ 50\,(\phi_{SV} - \phi_{SS})$$

$$+ \left(\frac{240}{749}\right) H_T(s)\,H_S(s)\exp(-\tau s)\,\phi_T \qquad (37)$$

where the transmitter phase error ϕ_T is that specified in Eq. (31). Comparing Eqs. (35) and (37), one notes that, as seen previously in the X/X analysis, the effects of Θ_A, ϕ_{UC}, ϕ_{CC}, and ϕ_{ES} will be significantly greater during actual spacecraft tracking than during testing. The effect of ϕ_{SV} and ϕ_{SS} will be the same during tests and actual tracking. Finally, assuming $H_T(s) = 1$ over the frequency band of interest, the Allen variance of the transmitter contribution to S-band doppler phase noise will be a factor of $(240/749)^2$ less during actual spacecraft tracking than during tests with the same transmitter mode.

V. Conclusion

Phase transfer functions between each phase error source and the X-band and S-band doppler extractor outputs for both the system configurations used during testing and those used during actual spacecraft tracking have been determined here. These results show that the contribution of the exciter frequency synthesizer phase error ϕ_{ES}, the hydrogen maser phase Θ_A, the compensated cable phase error ϕ_{CC} and the uncompensated cable phase error ϕ_{UC} to the X-band and S-band doppler phase errors will be very much less in test configurations than in actual spacecraft tracking. The primary reason for this difference is the two-way time delay in the tracking configuration. The contributions of the exciter-modulator phase error ϕ_{EM} and the RF power amplifier phase error ϕ_{PA} in the test configurations will be slightly less at X-band and significantly greater at S-band than during actual spacecraft tracking. The reason for this difference is that the transponder frequency "gains" are 880/749 for the X-band downlink and 240/749 for the S-band downlink, whereas the frequency "gains" of both the X-band and the S-band test translators, for the transmitter phase noises ϕ_{EM} and ϕ_{PA}, are unity. Finally, the contributions of the VCO and frequency synthesizer phase errors in both the X-band and S-band receivers will be the same during testing as during actual spacecraft tracking.

Given power spectra for the phase error sources, the transfer functions presented in this article can be used to calculate quantitative values instead of the qualitative observations presented above. The DSN station stability program will supply the measurements of the individual error sources. A subsequent article will compare the results obtained by combining the individual measurements, using the test mode phase transfer functions presented in this article, with the results from the end-to-end tests. This comparison is expected to aid in the understanding of the end-to-end test data and to either verify or suggest modifications to the preceding analysis.

Appendix

Exciter, X-Band Receiver, and S-Band Receiver Frequency Synthesizer Multiplication Factors

The exciter, X-band receiver, and S-band receiver frequency synthesizer multiplication factors (M_E, M_X, and M_S) will be adjusted to obtain the desired transmitter and receiver frequencies.

I. Exciter

The frequency of the transmitted RF signal (in MHz) will be

$$f_T = 6500 + 1600\,M_E \tag{A-1}$$

Thus,

$$M_E = \frac{(f_T - 6500)}{1600} \tag{A-2}$$

For f_T = 7162.3125 MHz, M_E = 0.4139453125.

II. X-Band Receiver

If f_{RX} is the center frequency (in MHz) of the X-band receiver,

$$50\,(100\,M_X - 21) - (f_{RX} - 8100) = 1050 \tag{A-3}$$

or

$$M_X = \frac{(f_{RX} - 6000)}{5000} \tag{A-4}$$

Since

$$f_{RX} = \left(\frac{880}{749}\right) f_T\,, \tag{A-5}$$

$$M_X = \frac{(1408\,M_E + 1226)}{3745} \tag{A-6}$$

For f_{RX} = (880/749) 7162.3125 MHz = 8415 MHz, M_X = 0.483.

III. S-Band Receiver

If f_{RS} is the center frequency (in MHz) of the S-band receiver,

$$50\,(100\,M_S - 21) - (f_{RS} - 2000) = 1050 \tag{A-7}$$

or

$$M_S = \frac{(f_{RS} + 100)}{5000} \tag{A-8}$$

Since

$$f_{RS} = \left(\frac{240}{749}\right) f_T \tag{A-9}$$

$$M_S = \frac{(3840\,M_E + 16349)}{37450} \tag{A-10}$$

For f_{RS} = (240/749) 7126.3125 MHz = 2295 MHz, M_S = 0.479.

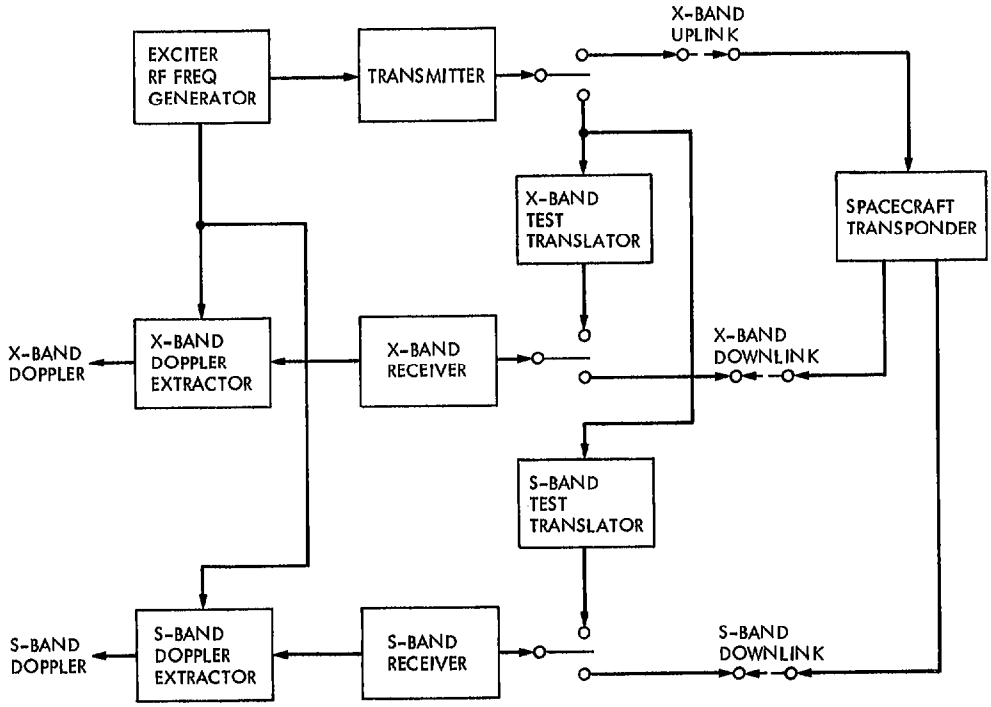

Fig. 1. (X/X, X/S) system functional block diagram

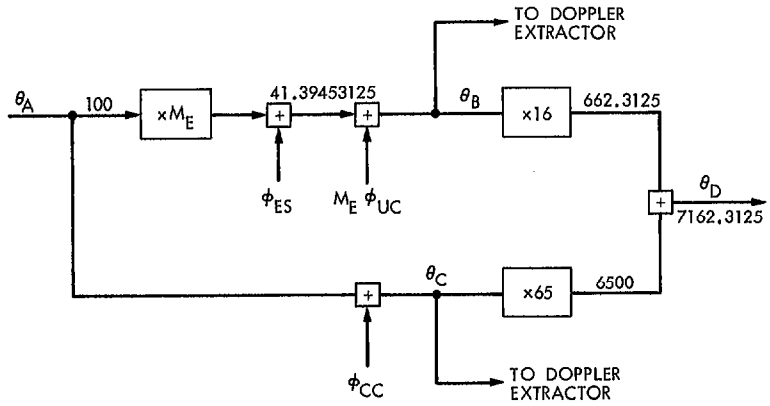

Fig. 2. Exciter RF frequency generator analytical model

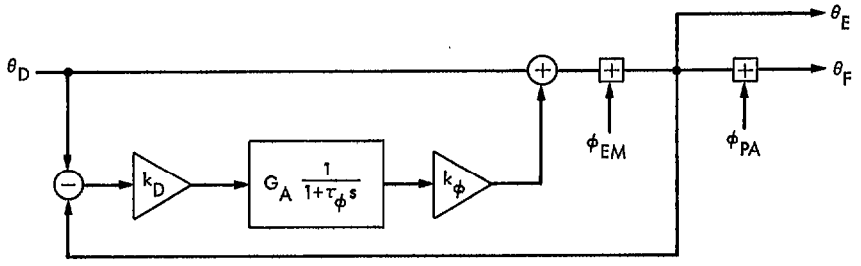

Fig. 3. Transmitter analytical model for feedback from the exciter output

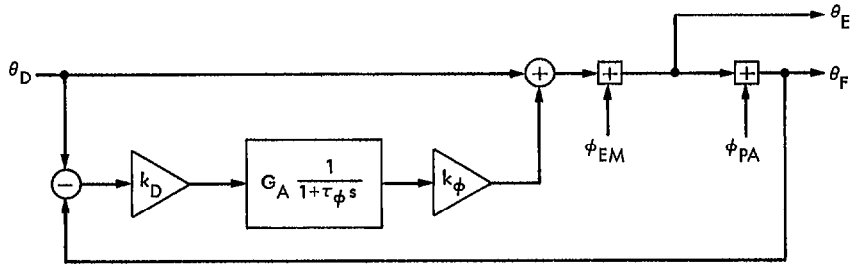

Fig. 4. Transmitter analytical model for feedback from the power amplifier output

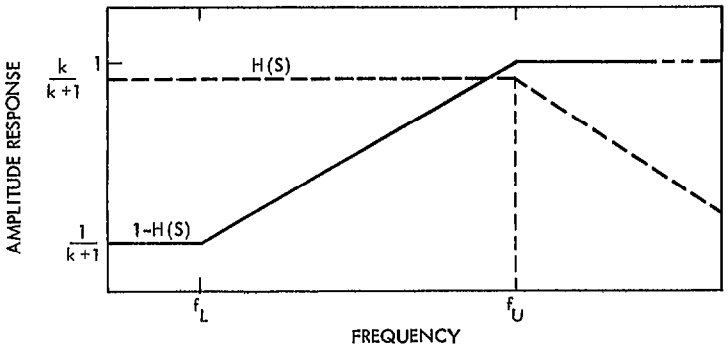

Fig. 5. Transmitter phase compensation loop amplitude responses

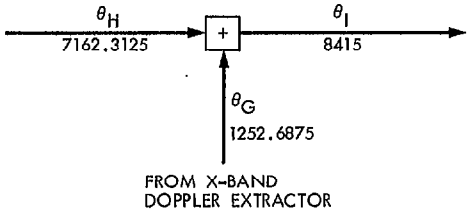

Fig. 6. X-band test translator analytical model

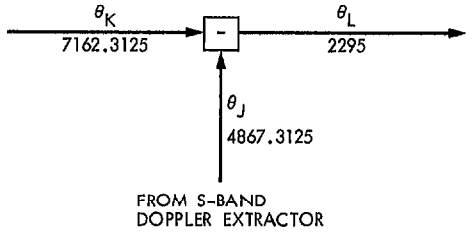

Fig. 7. S-band test translator analytical model

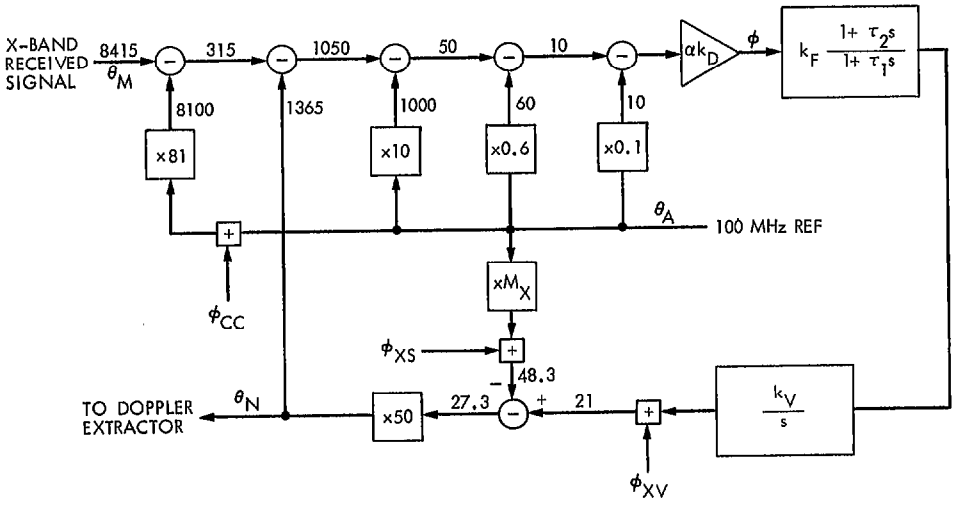

Fig. 8. X-band receiver analytical model

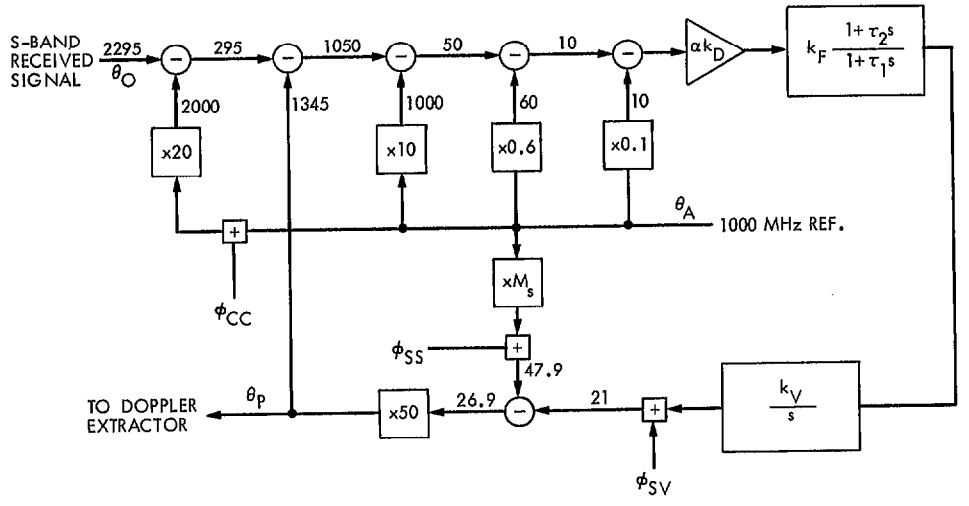

Fig. 9. S-band receiver analytical model

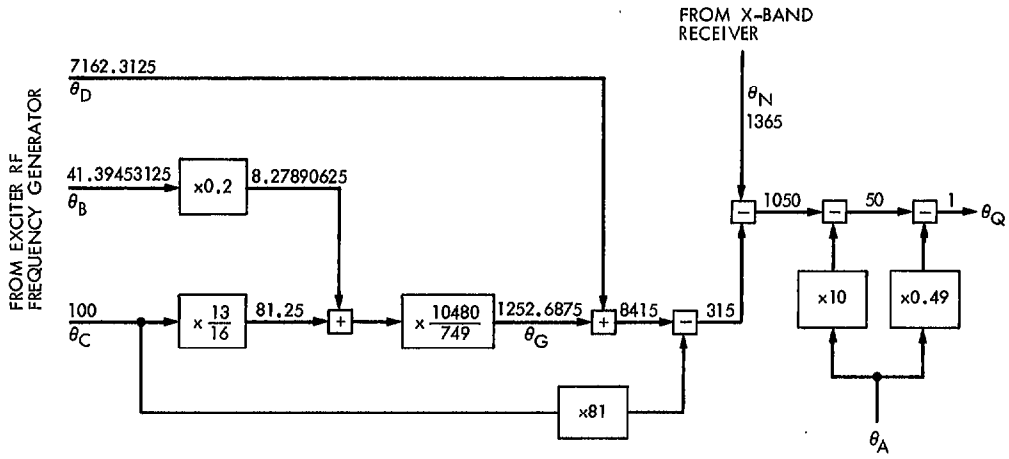

Fig. 10. X-band doppler extractor analytical model

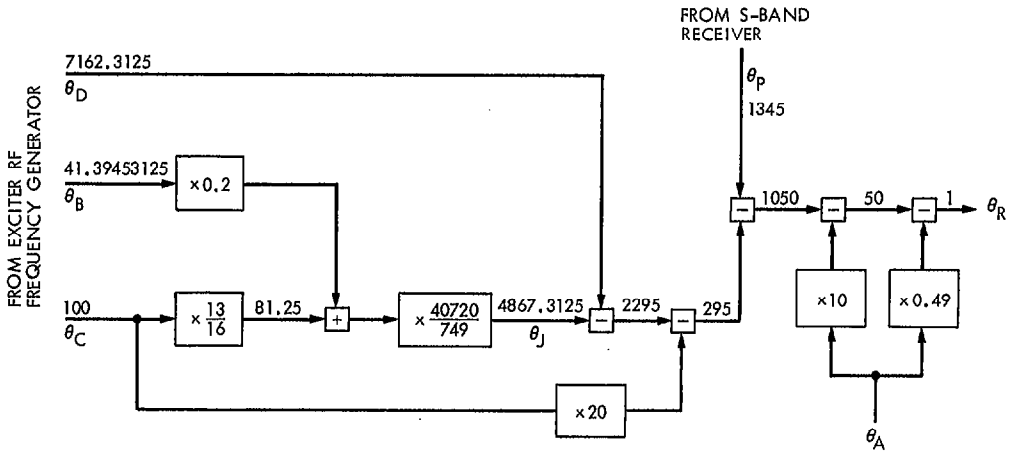

Fig. 11. S-band doppler extractor analytical model